

Scaling properties of viscous fingering

Bertrand Lagrée^{*1,2}, Stéphane Zaleski², Igor Bondino^{1,3},
Christophe Josserand², and Stéphane Popinet^{2,4}

¹TOTAL SA, Courbevoie, France

²Sorbonne Universités, UPMC Univ Paris 06, CNRS, UMR 7190,
Institut Jean le Rond d'Alembert, F-75005, Paris, France

³Centre Scientifique et Technique Jean F  ger, Pau, France

⁴National Institute of Water and Atmospheric Research,
Wellington, New Zealand

November 3, 2014

Abstract

We present a study of viscous fingering using the Volume Of Fluid method and a central injection geometry, assuming a Laplacian field and a simple surface tension law. As in experiments we see branched structures resulting from the Saffman-Taylor instability. We find that the area A of a viscous-fingering cluster varies as a simple power law $A \sim L^\alpha$ of its interface length L . Our results are compared to previously published simulations in which the viscosity of the invading fluid is vanishing. We find differences in exponent α and in the appearance of detached droplets and bubbles.

Saffman-Taylor's instability [1] is the result of the motion of two viscous fluids in the narrow space between two parallel plates known as a Hele-Shaw cell [2], for specific viscosity ratios. Indeed, when a fluid of lower viscosity displaces a fluid with a higher one, the interface between them becomes unstable and starts to deform. While the pressure field p satisfies the Laplace equation [3], the interface will move according to Darcy's law [4]. This problem is formally close both to Diffusion-Limited Aggregation (DLA) [5] and viscous flows in porous media [6, 7].

While Saffman and Taylor used a long and narrow rectangular channel, more recent works have considered radial [8, 9, 10] and wedge [11, 12] geometries, alongside the historical linear one [13, 14, 15], both experimentally and numerically. Because of the typical fingering observed in DLA [16, 17], porous media experiments [18, 19] and Hele-Shaw cells [20], interest has focused on the fractal aspect [21].

The Hausdorff dimension D_F of a fractal set is often determined by considering the density-density correlation function [22]. Indeed, this correlation function varies as $r^{-\delta}$ for small values of r in both viscous fingering and DLA in

^{*}blagree@dalembert.upmc.fr

circular geometry [23]. It is easy to demonstrate the exponent is closely related to the dimension of the considered fractal cluster. Sharon *et al.* [24] noticed that the fractal dimension of Saffman-Taylor fingering obtained with central injection was close to the one of circular DLA (both measured [23] and theoretical [25]).

As in references [9, 26], we study the development of Saffman-Taylor fingering in a Hele-Shaw cell with central injection in the presence of surface tension. For this purpose, we focus on two-dimensional (2D) square domains Ω of size L_d centered on $(0,0)$. The two components of the velocity are (u, v) , *i.e.*, $\mathbf{u} = u(x, y)\mathbf{e}_x + v(x, y)\mathbf{e}_y$. This domain is initially filled with a high-viscosity fluid ($\mu = 1$). A less viscous fluid ($\mu = M \ll 1$) is injected from the center of the domain with a constant massflux inside a circle of radius $0.8 \ll L_d$. The side boundaries ($x = \pm L_d/2$ and $y = \pm L_d/2$) impose a quasi-circular "free" outflow condition for the fluids with Neumann boundary conditions for the velocity: $\partial_x u(\pm L_d/2, y) = \partial_y v(x, \pm L_d/2) = 0$.

The fluids are considered incompressible ($\nabla \cdot \mathbf{u} = 0$) and move inside the domain according to Darcy's law:

$$\mathbf{u} = -(1/\mu)\nabla p. \quad (1)$$

Due to fluid incompressibility and equation (1), the pressure field p obeys the Laplace equation $\nabla^2 p = 0$ [3].

Boundary conditions are given at the interface which hold for the depth-averaged fields:

$$[\mathbf{n} \cdot \mathbf{u}] = 0, \quad (2a)$$

$$[p] = A + \lambda_\sigma/R. \quad (2b)$$

Here $[\]$ denotes a jump, R is the principal radius of curvature of the projection, onto the plane, of the tip of the meniscus separating the two phases and λ_σ a characteristic lengthscale of the influence of surface tension, multiplied by some coefficient of order 1 [27].

Let $c(x, y, t)$ be a marker function such that $c(x, y, t) = 1$ in fluid 1 (*i.e.* the invading fluid), and $c(x, y, t) = 0$ in fluid 2 (the receding one). The surface tension is given by $\mathbf{f}_\sigma = \kappa \delta_S \mathbf{n}$ where κ is the curvature and $\delta_S(x, y) = |\nabla c(x, y, t)|$ at the interface S in the distribution sense. By considering that \mathbf{n} points towards the invading fluid 1, one can write $\mathbf{n} = \nabla c/|\nabla c|$ and $\kappa = -\nabla \cdot \mathbf{n} = A + \lambda_\sigma/R$ according to equation (2b).

To consider surface tension, equation (1) should be written as:

$$\mathbf{u} = -(1/\mu) [\nabla p + \kappa(x, y, t) \delta_S \mathbf{n}] \quad (3a)$$

$$= -(1/\mu) [\nabla p + (A + \lambda_\sigma/R) \nabla c(x, y, t)]. \quad (3b)$$

Defining $p^* = p + Ac$ in equation (3b) allows to use only λ_σ/R in equation (2b) as the pressure jump due to surface tension [4].

Our model is implemented in GERRIS, a free-software solver for the solution of incompressible fluid motion using the finite-volume approach [28, 29]. Gerris uses the Volume-of-Fluid (VOF) method [30] to describe variable-density and/or variable-viscosity two-phase flows. In this method, the Euler equations are

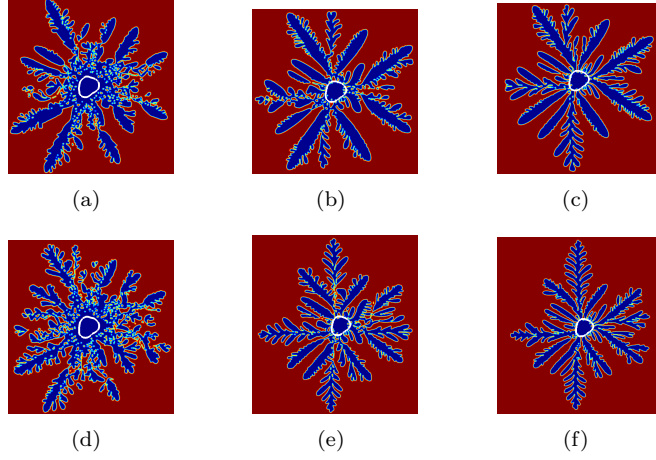


Figure 1: Development of Saffman-Taylor fingering for three different viscosity ratios: 10^{-2} (pictures (a) and (d)), 10^{-3} (pictures (b) and (e)), 10^{-4} (pictures (c) and (f)). The instability is generated by mesh-induced noise in the first row, while an isotropic noise is added to the simulations presented in the second row. In white, the initial position of the interface.

written as:

$$\rho(\partial_t \mathbf{u} + \mathbf{u} \cdot \nabla \mathbf{u}) = -\nabla p + \rho \mathbf{f}, \quad (4a)$$

$$\partial_t c + \nabla \cdot (c \mathbf{u}) = 0, \quad (4b)$$

$$\rho = \rho(c) = c\rho_1 + (1-c)\rho_2. \quad (4c)$$

The GERRIS flow solver can simulate Darcy flow [4, 31]. Here we also describe how to obtain the time dependent problem which was not considered in [4]. We cancel the advection term of (4a) and add a drag force $\mathbf{f} = -\mathbf{u} : \partial_t \mathbf{u} = -(1/\rho)\nabla p - \mathbf{u}$. We decompose the numerical solution into an exact and an error term: $\mathbf{u}(t) = \mathbf{u}_0 + \mathbf{e}(t)$ with $0 = -\nabla p - \rho \mathbf{u}_0$ for the exact term. The error \mathbf{e} obeys $\partial_t \mathbf{e} = -\mathbf{e}$ for a steady exact solution and is $\mathbf{e} = -\mathbf{C} \exp(-t)$. The error will be small after one timestep τ if $\tau \gg 1$. For a time-dependent exact solution \mathbf{u}_0 , the same decomposition shows that the error scales as \mathbf{u}_0/T_c where T_c is the (dimensionless) characteristic time of the exact solution and it thus requires that $T_c \gg 1$. The latter condition is achieved by the choice of length and time units. Thus the solver produces either a false-transient iteration towards the steady state or adiabatically follows the time-dependent solution of $\mathbf{u} = -(1/\rho)\nabla p$, which is equivalent to Darcy's law if $\rho = \mu$.

We simulate viscosity ratios $M = \mu_1/\mu_2$ from 10^{-4} to 10^{-2} . Using the pressure field p^* presented alongside equation (3b), we only consider the planar contribution to the radius of curvature.

The initial data is a slightly perturbed circular interface $r(\theta) = 1 + 1/10(\cos(3\theta) + \sin(2\theta))$ [9]. We only report on the early times $r_{\max}/L_d \ll 1$ to avoid finite-size effects and mesh-induced anisotropy. We fix $\lambda_\sigma = 1/3$ so that the capillary length scale is somewhat smaller than the initial radius r and the grid size is $h = 1/60$.

In related simulations (invasion from the side of a rectangular domain, to be

Viscosity ratio	10^{-2}	10^{-3}	10^{-4}
Mesh-induced noise	$1.79 \rightarrow 1.58$	$1.81 \rightarrow 1.60$	1.69
Added noise	$1.85 \rightarrow 1.56$	1.68	1.70

Table 1: Fractal dimensions of the clusters presented in Figure 1. When two different values are presented, the first one corresponds to the lower radii and the second one to the higher ones.

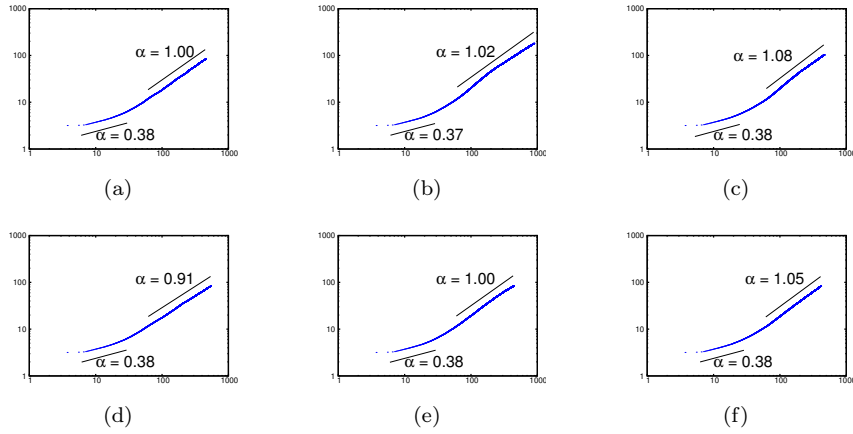


Figure 2: The dimensionless area A of the growing bubble *vs.* the dimensionless length L of the interface. The different viscosity ratios and noise origins are presented similarly to Figure 1.

reported in a following publication) we found that if care is taken to ensure very low noise levels fingering disappears and plain, non-branching fingers advance linearly. Thus our simulations incorporate two different kind of noise, numerical or “mesh-induced” noise (due mostly to the finite tolerance on the convergence of the Poisson solver) or random perturbations of the local viscosity (viscosity added noise). The early-time instability amplifies the initial perturbation, then later-time fingerings develop due to either mesh-induced noise [pictures 1(a) to 1(c)], or added noise [pictures 1(d) to 1(f), strong enough to cover the still-present mesh-induced noise]. In this last case, the noise is also axis-dependent, due to the non-isotropic distribution of computational grid points. The viscosity added noise has standard deviation $[\Delta(1/\mu)]/(< 1/\mu >) = 5\%$. It was added to try to account for the sensitivity of the fingering process to noise [32], for instance in porous media.

The error is due to several contributions: numerical uncertainty as stated above, mesh-size effects, finite-size effects (special care was taken to verify they are negligible: a specific flow was considered for several domain sizes L_d , resulting in convergence with an error lower than 2%), data range used to compute power-law fits, and quality of the fitting process for a specific data range.

At higher viscosity ratios patches are seen to detach from the main bubble. Moreover, some fingers tend to reconnect at later times, trapping some high viscosity droplets inside the less viscous main bubble [see pictures 1(a) and 1(d)]. On the contrary, for lower viscosity ratio, the different early-time fingers develop separately without uniting one with the other [no detaching droplets; pictures 1(c) and 1(f)]. These two different cases result in different fractal-dimension regimes, presented in Table 1 (fitting uncertainty always lower than 2%): at higher viscosity ratio, the inner (lower radii) fractal dimension is higher than the outer (higher radii) one (around 1.8 *vs.* around 1.6); on the contrary at lower viscosity ratio, there is only one fractal dimension for the whole bubble (around 1.7).

It can also be noted that the transition from the two-fractal-dimension regime (high viscosity ratio, see above and Table 1) to the one-fractal-dimension one (low viscosity ratio) occurs at higher viscosity ratio when the noise amplitude is higher. Logically, the higher the noise amplitude, the more pronounced the resulting fingering (see Figure 1).

When numerically simulating Saffman-Taylor fingering [33, 9], it is common to consider a constant pressure field p_0 inside the less viscous fluid (usually considered equal to zero). This is equivalent to the assumption of a zero-viscosity invading fluid. In this approximation and without surface tension, the pressure is p_0 everywhere on the interface. Due to the maximum principle (a consequence of the open-mapping theorem), the maximum pressure of a Laplacian field such as p in the domain occupied by the invaded, more viscous fluid is only reached at the domain boundary, here the interface. The maximum is thus p_0 and is reached at the interface, with $p < p_0$ everywhere else. Thus the interface can only advance towards the more viscous fluid and never recede. This makes the pinch-off of invading fluid bubbles impossible. The presence of detaching droplets is thus a qualitative difference with infinite viscosity contrast models.

In reference [9], Fast & Shelley explain that long-time simulations of Saffman-Taylor fingering reveal an asymptotic scaling regime, where the interface length of the resulting bubble is related to the bubble area by a power-law relation: $\text{Area} \sim (\text{Length})^{\alpha_\infty}$ (in their case, $\alpha_\infty = 1.45$). The variation of this coefficient

α is obviously disconnected from that of the fractal dimension D_F ; indeed, as an example, one can consider a lone planar dendrite whose length and width grow as t and t^γ respectively (with $0 < \gamma < 1$), then $D_F = 2$ whatever the value of γ whereas $\alpha_\infty = 1 + \gamma$. Approximating fingers by their osculating parabolas one gets $\gamma = 1/2$ and $\alpha_\infty = 3/2$. In the case of DLA clusters, $\alpha_\infty = 1$ whatever the fractal dimension.

Fast & Shelley [9] also found a short-time scaling with another coefficient $\alpha_1 = 0.61$. Li *et al.* [26] found similar results.

In Figure 2, we also find that the interface length is related to the bubble area by a power-law scaling with two different regimes. However, the coefficients that we obtain are different: $\alpha_1 \approx 0.38$, and $\alpha_\infty \approx 1$, depending on the viscosity ratio and noise origin. The error, mostly due to mesh-size effects, on all values of both α_1 and α_∞ is of order 10%. However oscillations in the scaling exponent are inherent to the self-similar character of the fingering [34] and could also account for part of the error.

It should also be noted that the coefficient α_∞ increases slightly when the viscosity ratio decreases, although we have not enough numerical data to further comment on the significance of this increase.

Due to the high discrepancy of coefficient values between our results and those of reference [9], both Fast & Shelley's results and ours were compared to the experimental results presented by Praud & Swinney in reference [35]. This comparison was realized cautiously, for, while our results and Fast & Shelley's were realized at constant massflux, Praud & Swinney's injection was realized at constant pressure. The experiments were also realized with the viscosity ratio $M \sim 5 \cdot 10^{-5}$, *i.e.*, close to what we used for pictures 2(c) and 2(f). At $M \sim 5 \cdot 10^{-5}$ in the experiments or $M \sim 10^{-4}$ in the simulation very few or even no detached bubbles or trapped droplets are seen, making this case similar to the $M = 0$ one.

From Figure 3, it was possible to determine $\alpha_\infty = 1.14$, with the following fitting error: $\alpha_\infty \in [1.11, 1.23]$. Our results ($\alpha_\infty \in [1.02, 1.08]$ with the fitting uncertainty resulting from data range), are much closer than those of Fast & Shelley.



Figure 3: Time evolution of the fractal growth patterns for viscous fingering ($\Delta p = 1.25$ atm). The colors indicate the ages of the patterns; the oldest (first created) region is blue and the youngest is red. From [35].

In order to completely validate our model, we simulated the experiment presented in Figure 3. The simulation was realized with a maximum number of authorized computational cells of 2^{13} in each direction with the same viscosity ratio as in Figure 3. As there was no blatant difference between the results of simulations obtained by applying a constant pressure (as in the experiment of Praud & Swinney) and those with a constant massflux, we present in Figure 4 the results realized with a constant massflux, for which a length λ_σ was defined above.

Though Figures 3 and 4 look very much alike, it is obvious that our fingers begin to align themselves with the principal directions of the mesh: the X-axis, the Y-axis and both bisectors of the axes.

We nonetheless determined the fractal dimension $D_F = 1.67$ of the resulting cluster, to be compared with $D_F = 1.69$ in Figure 3. For all we know, the fractal dimension of a Direct Numerical Simulation of Saffman-Taylor fingering was never measured beforehand.

As a conclusion, we observe the existence of two different regimes in Saffman-Taylor fingering due to central injection: one at higher viscosity ratio with the coexistence of two different fractal dimensions in the resulting cluster, and one at lower viscosity ratio with only one dimension. What is more, at late times, the area of the resulting bubble varies as the length of the interface to some power α_∞ , with α_∞ increasing with decreasing viscosity ratio.

Acknowledgments

We thank TOTAL for the financial support and permission to publish this study.

References

- [1] P. G. Saffman and Geoffrey I. Taylor. The penetration of a fluid into a porous medium or Hele-Shaw cell containing a more viscous fluid. *Proc. R. Soc. London*, 245(1242):312-329, 1958.
- [2] H. S. Hele-Shaw. Flow of water. *Nature*, 58:520, 1898.



Figure 4: Simulation of the experiment presented in [35] ($r_{\max}/\lambda_\sigma = 25$).

- [3] C. Tang. Diffusion-limited aggregation and the Saffman-Taylor problem. *Phys. Rev. A*, 31:1977–1979, March 1985.
- [4] S. Afkhami and Y. Renardy. A volume-of-fluid formulation for the study of co-flowing fluids governed by the Hele-Shaw equations. *Phys. Fluids*, 25(8):1–19, 2013.
- [5] T. A. Witten and L. M. Sander. Diffusion-Limited Aggregation, a Kinetic Critical Phenomenon. *Phys. Rev. Lett.*, 47:1400–1403, November 1981.
- [6] S. Whitaker. Flow in porous media I: A theoretical derivation of Darcy’s law. *Transport Porous Med.*, 1:3–25, 1986.
- [7] S. Whitaker. Flow in porous media II: The governing equations for immiscible, two-phase flow. *Transport Porous Med.*, 1:105–125, 1986.
- [8] J. Bataille. Stabilité d’un écoulement radial non miscible. In *Rev. I. Fr. Petrol.*, volume 23, page 1349, 1968.
- [9] P. Fast and M. J. Shelley. Moore’s law and the Saffman–Taylor instability. *J. Comput. Phys.*, 212(1):1 – 5, 2006.
- [10] S. Li, J. S. Lowengrub, J. Fontana, and P. Palffy-Muhoray. Control of Viscous Fingering Patterns in a Radial Hele-Shaw Cell. *Phys. Rev. Lett.*, 102:174501, Apr 2009.
- [11] R. Combescot and M. Ben Amar. Selection of Saffman-Taylor fingers in the sector geometry. *Phys. Rev. Lett.*, 67:453–456, July 1991.
- [12] A. Arneodo, J. Elezgaray, M. Tabard, and F. Tallet. Statistical analysis of off-lattice diffusion-limited aggregates in channel and sector geometries. *Phys. Rev. E*, 53:6200–6223, June 1996.
- [13] D. Bensimon. Stability of viscous fingering. *Phys. Rev. A*, 33:1302–1308, February 1986.
- [14] M. Rabaud, Y. Couder, and N. Gerard. Dynamics and stability of anomalous Saffman-Taylor fingers. *Phys. Rev. A*, 37:935–947, Feb 1988.
- [15] S. Tanveer. Surprises in viscous fingering. *J. Fluid Mech.*, 409:273–308, 2000.
- [16] T. A. Witten and L. M. Sander. Diffusion-limited aggregation. *Phys. Rev. B*, 27:5686–5697, May 1983.
- [17] L. M. Sander. Fractal growth processes. *Nature*, 322(6082):789–793, 1986.
- [18] J.-D. Chen and D. Wilkinson. Pore-Scale Viscous Fingering in Porous Media. *Phys. Rev. Lett.*, 55:1892–1895, October 1985.
- [19] K. J. Måløy, J. Feder, and T. Jøssang. Viscous Fingering Fractals in Porous Media. *Phys. Rev. Lett.*, 55:2688–2691, December 1985.
- [20] C.-W. Park and G. M. Homsy. The instability of long fingers in Hele–Shaw flows. *Phys. Fluids*, 28(6):1583–1585, 1985.

- [21] L. M. Sander. Fractal Growth Processes. In Robert A. Meyers, editor, *Mathematics of Complexity and Dynamical Systems*, pages 429–445. Springer New York, 2011.
- [22] P. Grassberger and I. Procaccia. Characterization of Strange Attractors. *Phys. Rev. Lett.*, 50:346–349, January 1983.
- [23] M. Conti, B. Meerson, and P. V. Sasorov. Breakdown of Scale Invariance in the Phase Ordering of Fractal Clusters. *Phys. Rev. Lett.*, 80:4693–4696, May 1998.
- [24] E. Sharon, M. G. Moore, W. D. McCormick, and H. L. Swinney. Coarsening of fractal viscous fingering patterns. *Phys. Rev. Lett.*, 91:205504, Nov 2003.
- [25] B. Davidovitch, A. Levermann, and I. Procaccia. Convergent calculation of the asymptotic dimension of diffusion limited aggregates: Scaling and renormalization of small clusters. *Phys. Rev. E*, 62:R5919–R5922, November 2000.
- [26] S. Li, J. S. Lowengrub, and P. H. Leo. A rescaling scheme with application to the long-time simulation of viscous fingering in a Hele–Shaw cell. *J. Comput. Phys.*, 225(1):554 – 567, 2007.
- [27] C.-W. Park and G. M. Homsy. Two-phase displacement in Hele Shaw cells: theory. *J. Fluid Mech.*, 139:291–308, 1 1984.
- [28] S. Popinet. Gerris: a tree-based adaptive solver for the incompressible Euler equations in complex geometries. *J. Comput. Phys.*, 190(2):572 – 600, 2003.
- [29] S. Popinet. An accurate adaptive solver for surface-tension-driven interfacial flows. *J. Comput. Phys.*, 228(16):5838 – 5866, 2009.
- [30] G. Tryggvason, R. Scardovelli, and S. Zaleski. *Direct Numerical Simulations of Gas-Liquid Multiphase Flows*. Cambridge University Press, 2011.
- [31] G. D. McBain. Simple example of groundwater flow following Darcy’s law. Test case on the Gerris website.
- [32] H. Thomé, R. Combescot, and Y. Couder. Controlling singularities in the complex plane: Experiments in real space. *Phys. Rev. A*, 41:5739–5742, May 1990.
- [33] P. Fast and M. J. Shelley. A moving overset grid method for interface dynamics applied to non-newtonian hele–shaw flow. *J. Comput. Phys.*, 195(1):117 – 142, 2004.
- [34] L. A. Smith, J.-D. Fournier, and E. A. Spiegel. Lacunarity and intermittency in fluid turbulence. *Phys. Lett. A*, 114(8–9):465 – 468, 1986.
- [35] O. Praud and H. L. Swinney. Fractal dimension and unscreened angles measured for radial viscous fingering. *Phys. Rev. E*, 72:011406, Jul 2005.